



Imaging EEG Extended Sources Based on Variation Sparsity with L_1 -norm Residual

Furong Xu, Ke Liu^(✉), Xin Deng, and Guoyin Wang

Chongqing Key Laboratory of Computational Intelligence,
Chongqing University of Posts and Telecommunications, Chongqing, China
liuke@cqupt.edu.cn

Abstract. Reconstructing the locations and extents of cortical activities accurately from EEG signals plays an important role in neuroscience research and clinical surgeries. However, due to the ill-posed nature of EEG source imaging problem, there exist no unique solutions for the measured EEG signals. Additionally, evoked EEG is inevitably contaminated by strong background activities and outliers caused by ocular or head movements during recordings. To handle these outliers and reconstruct extended brain sources, in this paper, we have proposed a robust EEG source imaging method, namely L_1 -norm Residual Variation Sparse Source Imaging (L_1 R-VSSI). L_1 R-VSSI employs the L_1 -loss for the residual error to alleviate the outliers. Additionally, the L_1 -norm constraint in the variation domain of sources is implemented to achieve globally sparse and locally smooth solutions. The solutions of L_1 R-VSSI is obtained by the alternating direction method of multipliers (ADMM) algorithm. Results on both simulated and experimental EEG data sets show that L_1 R-VSSI can effectively alleviate the influences from the outliers during the recording procedure. L_1 R-VSSI also achieves better performance than traditional L_2 -norm based methods (e.g., wMNE, LORETA) and sparse constraint methods in the original domain (e.g., SBL) and in the variation domain (e.g., VB-SCCD).

Keywords: EEG inverse problem · Variation sparseness · Outliers · ADMM

1 Introduction

Electroencephalogram (EEG) are widely used techniques in cognitive neuroscience and clinical surgeries due to their non-invasiveness and high temporal

Supported in part by the National Natural Science Foundation of China under Grants 61703065, 61876027. Chongqing Research Program of Application Foundation and Advanced Technology under Grant cstc2018jcyjAX0151, the Science and Technology Research Program of Chongqing Municipal Education Commission under Grant KJQN201800612 and KJQN201800638.

resolution. The task to reconstruct the corresponding cortical neural activities from EEG signals on the scalp surface is termed as EEG source imaging. Using EEG source imaging, we can estimate the extents and locations of brain active regions, which provide important auxiliary information for neuroscience research and medical treatments.

To reconstruct brain activities, the distributed source model divides the cerebral cortex into several triangular grids, each of which represents a dipole source [8]. The amplitude of each dipole source can be calculated by solving a linear inverse problem. However, the number of the candidate dipole sources largely outnumbered that of EEG sensors. Hence, the linear inverse problem is highly ill-posed, i.e., there are infinite source solutions to satisfy EEG signals. To obtain a unique solution, appropriate regularization operator is needed to narrow the solution space [8, 9, 16].

Typical EEG source imaging methods employ the L_2 -norm regularizer, such as the weighted minimum norm estimate (wMNE) [4] and the low-resolution electromagnetic tomography (LORETA) [11]. However, the estimations of L_2 -norm based methods are overly diffused and spread widely [8]. To improve the spatial resolution, sparse constrained methods based on L_p -norm ($0 < p \leq 1$) regularizer [1] and sparse Bayesian learning (SBL) [15] framework are developed. However, the solutions of conventional sparse constrained methods are too sparse and provide little information about source extents. To estimate the locations and extents of brain activities, several studies have proposed to implement sparse constraint on the transformed domains, such as the variation, wavelet and Laplacian domains [3, 5, 10, 16], which can provide more information about the source extents than the sparse constraints in the original source domains.

Most of the aforementioned methods assume that the measurement noise satisfies Gaussian distribution and employ the L_2 -norm to measure the residual error. Nevertheless, the EEG signals are inevitably contaminated by the strong background activities and outliers caused by ocular or head movements during recording procedure. The L_2 -norm may not be suitable to represent these outliers. To handle these outliers in the EEG signals and estimate the extended cortical activities, as in [1], we propose a robust EEG source imaging method, namely L_1 -norm Residual Variation Sparse Source Imaging (L_1 R-VSSI). L_1 R-VSSI employs the L_1 -norm to measure the residual error. In addition, to estimate the locations and extents of sources, L_1 R-VSSI attains sparseness of sources on the variation domain by incorporating the L_1 -norm constraint. The cortical sources of L_1 R-VSSI are efficiently obtained by the alternating direction method of multipliers (ADMM) algorithm [2].

The remaining of the paper is organized as follows. In Sect. 2, we present details of the proposed EEG source imaging algorithm. In Sect. 3, the simulation design and evaluation metrics are presented. Section 4 presents the results on simulated and real EEG data, followed by a brief conclusion in Sect. 5.

2 Methods

2.1 Background

The relationship between the EEG recordings and cortical sources can be expressed as [8]

$$\mathbf{b} = \mathbf{L}\mathbf{s} + \boldsymbol{\varepsilon} \tag{1}$$

where $\mathbf{b} \in \mathbb{R}^{d_b \times 1}$ is EEG recording, $\mathbf{s} \in \mathbb{R}^{d_s \times 1}$ is the unknown source vector. $\mathbf{L} \in \mathbb{R}^{d_b \times d_s}$ is the lead-field matrix that describes how a unit source of a certain candidate location is related to the EEG measurements. d_b and d_s denote the number of sensors and candidate sources respectively. $\boldsymbol{\varepsilon}$ denotes the measurement noise vector.

To estimate the extents and locations of sources, as in [5, 10], we assume that the sources are sparse in the variation domain. Each element in the variation domain is the difference of amplitudes between two adjacent dipole sources. When the amplitudes of sources are uniform, the non-zero vales of the variation sources are largely expected to occur on the boundaries between the active and inactive areas. Hence, we can estimate the sparseness on the variation domain to obtain the extents and locations of cortical activities. To obtain the variation sources, a variation operator $\mathbf{V} \in \mathbb{R}^{P \times d_s}$ is defined as [5, 10]

$$\mathbf{V} = \begin{bmatrix} v_{11} & v_{12} & \cdots & v_{1d_s} \\ v_{21} & v_{22} & \cdots & v_{2d_s} \\ \vdots & \vdots & \ddots & \vdots \\ v_{P1} & v_{P2} & \cdots & v_{Pd_s} \end{bmatrix} \tag{2}$$

$$\begin{cases} v_{pi} = 1, v_{pj} = -1, i < j; \text{ if source } i, j \text{ share edge } p \\ v_{pi} = 0; \text{ otherwise} \end{cases}$$

where P denotes the number of edges of triangular grids, which are defined by the source model. The p th row of \mathbf{V} corresponds to edge p . For each row of \mathbf{V} , only two elements corresponding to the two dipoles that share edge p are non-zero (i.e., 1, -1). The p th row of the variation sources $\mathbf{u} = \mathbf{V}\mathbf{s} \in \mathbb{R}^{P \times 1}$, u_p , indicates the difference of dipoles that share the p th edge.

2.2 L_1 R-VSSI: L_1 -norm Residual Variation Sparse Source Imaging

Usually, the EEG measurement noise $\boldsymbol{\varepsilon}$ is assumed to satisfy Gaussian distribution. And the fitting error is measured by the L_2 -norm for most EEG source imaging methods. However, the EEG signals are inevitably influenced by the artifacts induced by the head movement or eye blinks. The L_2 -norm for the fitting error will exaggerates the effect of these outliers. To handle these outliers or artifacts in EEG, our proposed EEG source imaging method, L_1 R-VSSI, employs the L_1 -norm to measure the fitting error. Combining the variation sparse constraint, the solution of L_1 R-VSSI is obtained as

$$\hat{\mathbf{s}} = \arg \min_{\mathbf{s}} \|\mathbf{L}\mathbf{s} - \mathbf{b}\|_1 + \lambda \|\mathbf{V}\mathbf{s}\|_1 \tag{3}$$

where $\lambda > 0$ is the regularization parameter. In this work, the ADMM algorithm is employed to solve formulation (3).

We first rewrite Eq. (3) as

$$\begin{aligned} \hat{\mathbf{s}} &= \arg \min_{\mathbf{s}} \|\mathbf{e}\|_1 + \lambda \|\mathbf{u}\|_1 \\ \text{s.t.}, \quad \mathbf{e} &= \mathbf{L}\mathbf{s} - \mathbf{b}, \mathbf{u} = \mathbf{V}\mathbf{s} \end{aligned} \quad (4)$$

Then the augmented Lagrangian function of the constrained optimization problem (4) is

$$\begin{aligned} \mathcal{L}(\mathbf{s}, \mathbf{e}, \mathbf{u}, \mathbf{y}, \mathbf{z}) &= \|\mathbf{e}\|_1 + \lambda \|\mathbf{u}\|_1 + \mathbf{y}^\top (\mathbf{L}\mathbf{s} - \mathbf{b} - \mathbf{e}) + \frac{\rho_1}{2} \|\mathbf{L}\mathbf{s} - \mathbf{b} - \mathbf{e}\|_2^2 \\ &+ \mathbf{z}^\top (\mathbf{V}\mathbf{s} - \mathbf{u}) + \frac{\rho_2}{2} \|\mathbf{V}\mathbf{s} - \mathbf{u}\|_2^2 \end{aligned} \quad (5)$$

where $\rho_1 > 0$ and $\rho_2 > 0$ are penalty parameters, $\mathbf{y} \in \mathbb{R}^{d_b \times 1}$ and $\mathbf{z} \in \mathbb{R}^{P \times 1}$ are the Lagrangian multipliers. Since \mathcal{L} is separable with respect the variables $(\mathbf{s}, \mathbf{e}, \mathbf{u})$, we can obtain $(\mathbf{s}, \mathbf{e}, \mathbf{u})$ with three subproblems.

$$\begin{aligned} \hat{\mathbf{s}}^{(k+1)} &= \arg \min_{\mathbf{s}} \mathcal{L} \left(\mathbf{s}, \mathbf{e}^{(k)}, \mathbf{u}^{(k)}, \mathbf{y}^{(k)}, \mathbf{z}^{(k)} \right) \\ &= \left(\rho_1 \mathbf{L}^\top \mathbf{L} + \rho_2 \mathbf{V}^\top \mathbf{V} \right)^{-1} \left[\rho_1 \mathbf{L}^\top \left(\mathbf{b} + \mathbf{e}^{(k)} \right) \right. \\ &\quad \left. + \rho_2 \mathbf{V}^\top \mathbf{u}^{(k)} - \mathbf{L}^\top \mathbf{y}^{(k)} - \mathbf{V}^\top \mathbf{z}^{(k)} \right] \end{aligned} \quad (6)$$

$$\begin{aligned} \hat{\mathbf{e}}^{(k+1)} &= \arg \min_{\mathbf{e}} \mathcal{L} \left(\mathbf{s}^{(k+1)}, \mathbf{e}, \mathbf{u}^{(k)}, \mathbf{y}^{(k)}, \mathbf{z}^{(k)} \right) \\ &= \mathcal{S}_{\frac{1}{\rho_1}} \left(\mathbf{L}\mathbf{s}^{(k+1)} - \mathbf{b} + \frac{1}{\rho_1} \mathbf{y}^{(k)} \right) \end{aligned} \quad (7)$$

$$\begin{aligned} \hat{\mathbf{u}}^{(k+1)} &= \arg \min_{\mathbf{u}} \mathcal{L} \left(\mathbf{s}^{(k+1)}, \mathbf{e}^{(k+1)}, \mathbf{u}, \mathbf{y}^{(k)}, \mathbf{z}^{(k)} \right) \\ &= \mathcal{S}_{\frac{1}{\rho_2}} \left(\mathbf{V}\mathbf{s}^{(k+1)} + \frac{1}{\rho_2} \mathbf{z}^{(k)} \right) \end{aligned} \quad (8)$$

where $\mathcal{S}_\kappa(a)$ is

$$\mathcal{S}_\kappa(a) = \begin{cases} a - \kappa, & a > \kappa \\ 0, & |a| < \kappa \\ a + \kappa, & a < -\kappa \end{cases} \quad (9)$$

The Lagrangian multipliers \mathbf{y} , \mathbf{z} are updated using the dual ascent method [2]

$$\hat{\mathbf{y}}^{(k+1)} = \mathbf{y}^{(k)} + \rho_1 (\mathbf{L}\mathbf{s}^{(k+1)} - \mathbf{b} - \mathbf{e}^{(k+1)}) \quad (10)$$

$$\hat{\mathbf{z}}^{(k+1)} = \mathbf{z}^{(k)} + \rho_2 (\mathbf{V}\mathbf{s}^{(k+1)} - \mathbf{u}^{(k+1)}) \quad (11)$$

where $\mathbf{x}^{(k)}$ is the value of x at k th iteration.

In summary, to obtain the source estimations, L_1 R-VSSI alternatively updates the variables $(\mathbf{s}, \mathbf{e}, \mathbf{u})$ and the Lagrangian multipliers (\mathbf{y}, \mathbf{z}) , until the

relative change of \mathbf{s} reaches a user-specified tolerance (e.g., 10^{-4}). Through our simulations, \mathbf{e} , \mathbf{u} , \mathbf{y} , \mathbf{z} are all initialized to $\mathbf{0}$. The penalty parameters ρ_1 , ρ_2 are determined by cross-validation [14]. For the simulation experiment of $d_s = 6002$, $d_b = 62$, $P = 17977$, it reaches convergence after approximately 200 iterations, which takes about 2 min.

3 Simulation Design and Evaluation Metrics

To test the performance of L_1 R-VSSI, a series of Monte-Carlo numerical simulations were set up to compare L_1 R-VSSI and four imaging methods: two widely used L_2 -norm based methods, i.e., wMNE [4] and LORETA [11], and sparse constraint methods in the original domain (SBL [15]) and in the variation domain (variation-based sparse cortical current density (VB-SCCD) [5]). Additionally, L_1 R-VSSI was also applied to one real clinical EEG data.

3.1 Simulation Design

In the numerical simulations, a three-shell head model is obtained using Brainstorm [13]. There are 6002 triangle grids evenly distributed on the cortical surface, each of which is a dipole source. The dipole orientation is fixed to be normal to the cortical surface. The lead-field matrix \mathbf{L} was constructed using Brainstorm with the sensor configuration of the 64-channel Neuroscan Quik-cap system (two channels are not EEG electrodes, hence, $\mathbf{L} \in \mathbb{R}^{62 \times 6002}$).

A triangle grid is randomly selected as a seed point. The adjacent triangles are gradually added to form an extended source. After multiplying the source vector with the lead-field matrix, the cortical activities are transformed into EEG electrode recordings. To simulate the actual EEG signals, both Gaussian noise and outliers are added to the EEG electrode recordings. The noise level is described by signal-to-noise ratio (SNR), which is defined as $\text{SNR} = 10 \log_{10} \left[\frac{\sigma^2(\mathbf{L}\mathbf{s})}{\sigma^2(\boldsymbol{\varepsilon})} \right]$, where $\mathbf{L}\mathbf{s}$ is raw EEG data without noise and $\boldsymbol{\varepsilon}$ is mixture measurement noise (Gaussian and outliers). $\sigma^2(\mathbf{x})$ is the variance of \mathbf{x} .

As in [1], the mixture measurement noise is defined as

$$\boldsymbol{\varepsilon} = \frac{\boldsymbol{\varepsilon}_1}{\sigma(\boldsymbol{\varepsilon}_1)} \left[10^{(-\frac{\text{SNR}}{20})} \right] \sigma(\mathbf{L}\mathbf{s}) \tag{12}$$

where $\boldsymbol{\varepsilon}_1$ denote the outliers and σ is the standard deviation.

To generate the mixture noise, we first generate the outliers $\boldsymbol{\varepsilon}_1 \in \mathbb{R}^{d_b \times 1}$, where each element of $\boldsymbol{\varepsilon}_1$ obeys Gaussian distribution $\mathcal{N}(\mu + 10\sigma^2, \sigma^2)$ [1]. μ and σ^2 are the mean and variance of the true EEG $\mathbf{L}\mathbf{s}$ across all channels at the single time slice, respectively. Then, given a specified SNR, the mixture noise is generated by Eq. (12) and added to the true EEG recordings $\mathbf{L}\mathbf{s}$.

In the numerical Monte-Carlo experiments, the performance of the proposed method are verified in two cases: (1) One extended source with different extents (i.e., 0.8, 4, 8, 12, 18 cm²); (2) EEG signals with different SNRs (i.e., 0, 5, 10, 15 dB). For each case, 100 simulation experiments were conducted to ensure that the simulated extended sources could cover most areas of the brain.

3.2 Evaluation Metrics

The performance of imaging algorithms are evaluated by four evaluation metrics. (1) The area under the receiver operating characteristic (ROC) curve (AUC), which assesses the sensitivity and specificity of imaging algorithms [7]; (2) Spatial dispersion (SD), which depicts that the level of the spatial dispersion of reconstructed source [3]; (3) Distance of localization error (DLE), which describes the location error of the estimated source activities [16]; (4) Relative mean square error (RMSE), which estimates the amplitudes accuracy of the reconstructed sources [9]. Larger AUC, smaller SD, DLE and RMSE values indicate that the method has better performance. The detailed computation of these metrics can refer to the supplementary document in [10]. To image the estimated sources, the absolute value of the recovered sources at specified time points are shown, thresholded by the Otsu’s method [7,10].

4 Results

4.1 Results for Various Extents

Figure 1 shows performance metrics under different extents. As the source extents increases, the AUC values of wMNE, SBL, VB-SCCD, L_1 R-VSSI gradually decrease. In contrast, LORETA’s AUC value increases, indicating the potential of LORETA to estimate large extents’ sources. The SD, DLE, RMSE values of wMNE, LORETA, VB-SCCD and L_1 R-VSSI gradually reduced, but L_1 R-VSSI get the smallest values, which means that L_1 R-VSSI have more accurate reconstructed solutions, smaller spatial dispersion and location errors. Due to the sparse constraint of SBL, although it gets the smallest SD, DLE values, its overly focal results also lead to a gradually increasing RMSE value. Comprehensively comparing the results of four evaluation metrics, the L_1 R-VSSI method shows better performance than the other four methods under different source extents.

Figure 2 depicts the imaging maps of reconstructed sources under different extents. The first column in Fig. 2 shows the simulated extended sources, and the remaining columns show the reconstructed sources estimated by the five imaging methods respectively. From the Fig. 2, we can see that SBL can reconstruct the focal sources perfectly. However, for large extents’ sources, it can only accurately locate the center of the sources, but the estimated extents are overly focused. In contrast, the solutions of wMNE and LORETA are too blurred compared to the simulated sources. Because the addition of variation operator, the blurriness of the imaging results of VB-SCCD solution is greatly reduced and more sensitive to the extents of the simulated sources. Nevertheless, compared to VB-SCCD, L_1 R-VSSI approach’s recovered solutions have more precise description for extents and strengths. This is because the use of L_1 -loss of the residual error reduces the influence of artificial noise. Combining the results of Figs. 1 and 2, L_1 R-VSSI performs better than wMNE, LORETA, SBL and VB-SCCD.

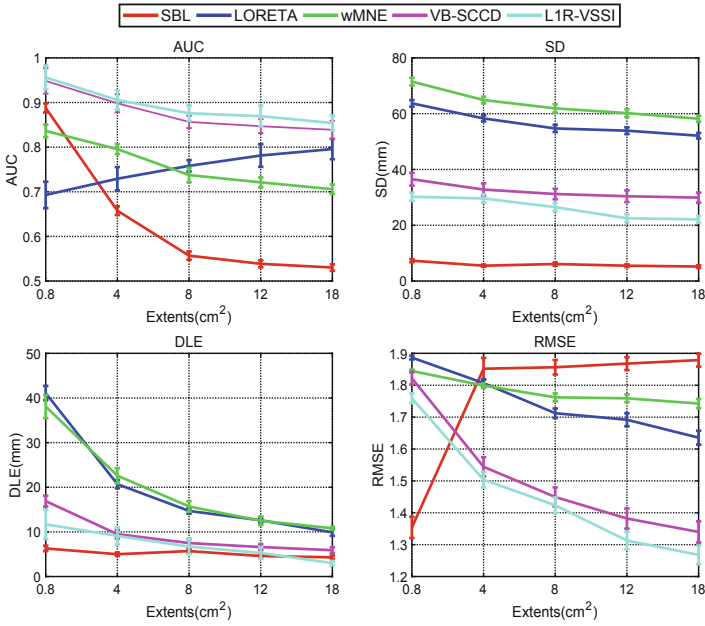


Fig. 1. Evaluation metrics of different source extents. The data is the results of 100 Monte Carlo simulations and is described as Mean \pm SEM (SEM: standard error of mean). The SNR is 5 dB.

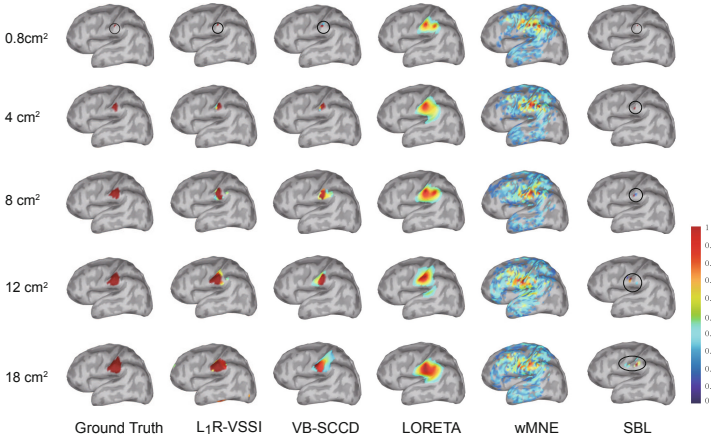


Fig. 2. Imaging results for different extents of extended sources. Source activity maps show the absolute value of the extended sources' activities. The threshold is determined using Otsu's method. The SNR is 5 dB. Some sources are circled for illustration purposes.

4.2 Results for Different SNRs

Figure 3 shows the performance evaluation metrics under different SNRs (0, 5, 10, 15 dB). All algorithms are significantly affected by the noise level. As the SNR increases, these algorithms' AUC value gradually increases, and the RMSE, SD, and DLE value decrease. Under comprehensive comparison, L_1 R-VSSI has a larger AUC value, smaller SD, RMSE, DLE value, so the performance is better than other approaches.

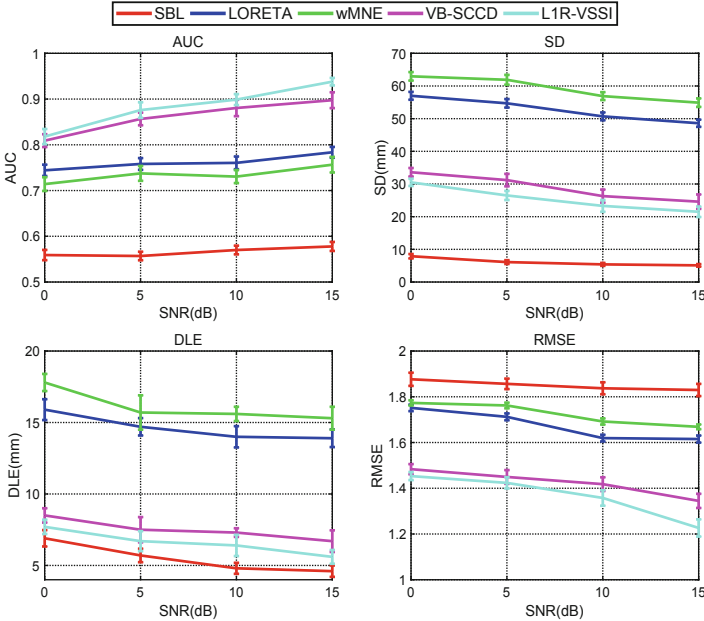


Fig. 3. Evaluation metrics of various SNRs. The data is the results of 100 Monte Carlo simulations and is described as Mean \pm SEM (SEM: standard error of mean). The extents of source is about 8 cm².

4.3 Application of Epilepsy EEG Data

To show the practical performance of L_1 R-VSSI, we further apply the proposed method to the Brainstorm public epilepsy data¹. The average spikes across 58 trials is used to estimate sources, which are presented in Fig. 4(a). We calculate the lead-field matrix based head model obtained from the head anatomical structure of the subject. The EEG data was collected from a patient who suffered from focal epilepsy with focal sensory, dyscognitive and secondarily generalized seizures since the age of eight years. After the resection of the epileptogenic area,

¹ <https://neuroimage.usc.edu/brainstorm/DatasetEpilepsy>.

postoperative investigation showed the patient no epilepsy in 5 years. In [6], it has located that the patient’s epileptogenic area is left frontal, which was estimated by invasive EEG. Figure 4(b) shows the imaging results of various algorithms at the peak time point (i.e., 0s). Comparing the results in Fig. 4(b) with the analysis in [6], we can find that these algorithms all locate the epileptogenic area. However, the epileptogenic area identified by LORETA and wMNE are overly diffused, even covering many other areas of the brain scalp. Conversely, SBL can only obtain some point sources in the epileptogenic area. For the variation sparse constraint based methods, the estimations by L_1R -VSSI and VB-SCCD is well accordant with previous reports [6, 12]. However, the solution of L_1R -VSSI shows more clear boundaries than that of VB-SCCD.

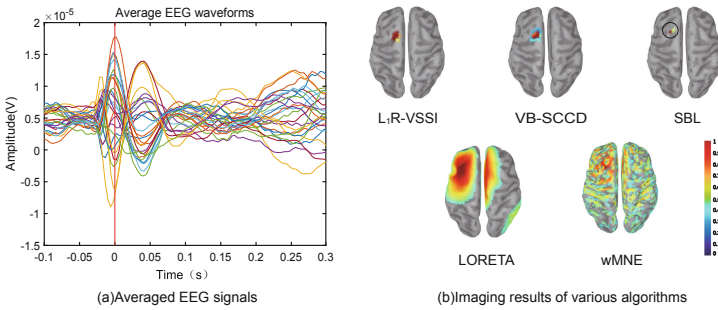


Fig. 4. Application of the public epilepsy data. (a) is averaged EEG signals across 58 trials. (b) is the imaging maps, showing the absolute value of the source activities at the peak time point. The imaging threshold was determined by Otsu’s method. SBL’s estimation is circled for illustration purposes.

5 Conclusions

We have proposed a robust EEG source estimation algorithm, L_1R -VSSI, which reconstructs extended sources using L_1 -loss of the residual error and sparse constraints in the variation domains. The solution of L_1R -VSSI is efficiently obtained by ADMM. Numerical results indicate that L_1R -VSSI can effectively alleviate the influence of outliers and achieves better performance (larger AUC value and smaller SD, DLE, RMSE value) than wMNE, LORETA, SBL and VB-SCCD in terms of reconstructing extended sources. However, due to page limit, for the experimental data analysis, we only applied L_1R -VSSI to analyze the epilepsy EEG data from Brainstorm. In our future work, we will also apply the proposed method to more clinical data to verify the performance, which will promote the development of neuroscience research and clinical medicine. Additionally, since the minimization of sources in the variation domain does not limit the global energy, L_1R -VSSI tends to underestimate the amplitude of sources [10, 16]. Our future work will also consider adding regularizers in other transform domains to improve the accuracy of amplitude.

References

1. Bore, J.C., et al.: Sparse EEG source localization using LAPPS: least absolute l-P ($0 < p < 1$) penalized solution. *IEEE Trans. Biomed. Eng.* **66**, 1927–1939 (2018)
2. Boyd, S., Parikh, N., Chu, E., Peleato, B., Eckstein, J., et al.: Distributed optimization and statistical learning via the alternating direction method of multipliers. *Found. Trends® Mach. Learn.* **3**(1), 1–122 (2011)
3. Chang, W.T., Nummenmaa, A., Hsieh, J.C., Lin, F.H.: Spatially sparse source cluster modeling by compressive neuromagnetic tomography. *Neuroimage* **53**(1), 146–160 (2010)
4. Dale, A.M., Sereno, M.I.: Improved localizadon of cortical activity by combining EEG and MEG with MRI cortical surface reconstruction: a linear approach. *J. Cognit. Neurosci.* **5**(2), 162–176 (1993)
5. Ding, L.: Reconstructing cortical current density by exploring sparseness in the transform domain. *Phys. Med. Biol.* **54**(9), 2683–2697 (2009)
6. Dümpelmann, M., Ball, T., Schulze-Bonhage, A.: sLORETA allows reliable distributed source reconstruction based on subdural strip and grid recordings. *Hum. Brain Mapp.* **33**(5), 1172–1188 (2012)
7. Grova, C., Daunizeau, J., Lina, J.M., Bénar, C.G., Benali, H., Gotman, J.: Evaluation of EEG localization methods using realistic simulations of interictal spikes. *Neuroimage* **29**(3), 734–753 (2006)
8. He, B., Sohrabpour, A., Brown, E., Liu, Z.: Electrophysiological source imaging: a noninvasive window to brain dynamics. *Annu. Rev. Biomed. Eng.* **20**, 171–196 (2018)
9. Liu, K., Yu, Z.L., Wu, W., Gu, Z., Li, Y., Nagarajan, S.: Bayesian electromagnetic spatio-temporal imaging of extended sources with Markov random field and temporal basis expansion. *Neuroimage* **139**, 385–404 (2016)
10. Liu, K., Yu, Z.L., Wu, W., Gu, Z., Li, Y., Nagarajan, S.: Variation sparse source imaging based on conditional mean for electromagnetic extended sources. *Neurocomputing* **313**, 96–110 (2018)
11. Pascual-Marqui, R.D., Michel, C.M., Lehmann, D.: Low resolution electromagnetic tomography: a new method for localizing electrical activity in the brain. *Int. J. Psychophysiol.* **18**(1), 49–65 (1994)
12. Sohrabpour, A., Lu, Y., Worrell, G., He, B.: Imaging brain source extent from EEG/MEG by means of an iteratively reweighted edge sparsity minimization (IRES) strategy. *Neuroimage* **142**, 27–42 (2016)
13. Tadel, F., Baillet, S., Mosher, J.C., Pantazis, D., Leahy, R.M.: Brainstorm: a user-friendly application for MEG/EEG analysis. *Comput. Intell. Neurosci.* **2011**, 8:1–8:13 (2011)
14. Wen, F., Pei, L., Yang, Y., Yu, W., Liu, P.: Efficient and robust recovery of sparse signal and image using generalized nonconvex regularization. *IEEE Trans. Comput. Imaging* **3**(4), 566–579 (2017)
15. Wipf, D., Nagarajan, S.: A unified Bayesian framework for MEG/EEG source imaging. *Neuroimage* **44**(3), 947–966 (2009)
16. Zhu, M., Zhang, W., Dickens, D.L., Ding, L.: Reconstructing spatially extended brain sources via enforcing multiple transform sparseness. *Neuroimage* **86**, 280–293 (2014)